Chinese Chemical Letters 33 (2022) 1589–1594

Contents lists available at ScienceDirect

Chinese Chemical Letters

journal homepage: www.elsevier.com/locate/cclet

A near-infrared multifunctional fluorescent probe for hypoxia monitoring and tumor-targeted therapy

Yuxun Lu[a,1], Jiajia Xu[b,1], Zongyun Jia[a], Siyu Kong[a], Yimu Qiao[a], Lin Li[b], Qiong Wu[b,*], Ying Zhou[a,1,*]

[a] College of Chemical Science and Technology, Yunnan University, Kunming 650091, China
[b] Key Laboratory of Flexible Electronics (KLOFE) & Institute of Advanced Materials (IAM), Jiangsu National Synergetic Innovation Center for Advanced Materials (SICAM), Nanjing Tech University (NanjingTech), Nanjing 211816, China

ARTICLE INFO

Article history:
Received 5 July 2021
Revised 1 September 2021
Accepted 1 September 2021
Available online 8 September 2021

Keywords:
Azoreductase
Hypoxia
Theranostic
Tumor

ABSTRACT

Hypoxia is one of the key characteristics of solid tumors. The over-expression of azoreductase resulting from hypoxia can be used as a target to visualize hypoxic levels and a trigger of the drug release system in tumor treatment. In this work, we developed a near-infrared fluorescent probe YLOD, composed of a near-infrared fluorophore, an azo bond, and an analogue of the anti-tumor drug melphalan. In the presence of azoreductase, YLOD displayed a red emission at 620 nm and released the anti-tumor drug concomitantly, thus achieving the integrated effects of hypoxic imaging and tumor treatment. Furthermore, YLOD successfully inhibited the growth of solid tumors during the tumor suppression experiments in nude mice. Considering all the results, YLOD emerges as a new fluorescence tool that can quickly determine the location and the edges of a tumor, showing concrete potential in clinical cancer treatment.

The tumor is, so far, one of the most threatening diseases to human life and health, involving uncontrolled cell growth and division [1,2]. The existing surgical resection is still the mainstream method in tumor treatments. As the boundary between tumor and normal tissue is difficult to assess through naked eyes, many excellent fluorescent probes have been developed for naked-eye recognition of solid tumors during surgery in recent years [3–5]. In 2021, Qin *et al*. reported a near-infrared ratiometric fluorescence probe TP-1 that can monitor tumors in mice by detecting pyroglutamate aminopeptidase 1 (PGP-1) [6]. Ma *et al*. developed a near-infrared fluorescence probe BHXP for tumor monitoring, composed of biotin as a tumor target group and triaryl phosphonate as an HNO sensing group [7]. Still, finding more tumor expression markers as recognition groups is imperatively demanding.

In tumors, the angiogenesis level cannot support fast tumor growth, limiting the oxygen supply and forming anoxic regions [8,9]. Thus, hypoxia becomes a characteristic property and plays a major role in the development of tumor cells [10,11]. Along with the enhanced invasiveness and metastasis, hypoxia also leads to higher expression of many enzymes in tumor cells than in normal tissues, mainly including nitroreductase, azoreductase, and diaphorase [12]. In 2017, our group developed a series of highly selective fluorescent probes using nitroreductase as a specific target for detecting hypoxia in cells and murine tumor models [13,14]. As researchers focused comprehensively on the integration of diagnosis and treatment [15], the importance of the release of therapeutic drugs and tumor monitoring simultaneously have been realized, leading to the emergence of many promising multifunctional fluorescent probes that consist of a fluorophore, connecting linker and active anti-cancer drug [16,17].

Azoreductase, a prevalent reductase in hypoxic tumors, shows lower expression levels in most healthy tissues [18,19]. In tumors, its concentration is directly related to the degree of hypoxia. Moreover, with the reduced form of nicotinamide adenine dinucleotide (NADH) acting as an electron donor, azoreductase can reduce and cause bond breaking of an azo group [20]. Considering the above two facts, by monitoring the concentration changes of azoreductase, the degree of hypoxia in the tumor can be established directly to determine tumor location and edges. In 2019, our group reported an azo-based hypoxia-responsive multifunctional fluorescent probe AzP1, which contained food and drug administration (FDA) approved anti-tumor drug SN-38 (irinotecan analogue) as a therapeutic drug, with a potential for both tumor hypoxia-specific activation and therapy [21]. With progressing research in this field, the requirement for dynamic tracking of the targeted drug deliv-

* Corresponding authors.
E-mail addresses: iamqwu@njtech.edu.cn (Q. Wu), yingzhou@ynu.edu.cn (Y. Zhou).
[1] These authors contributed equally to this work.

https://doi.org/10.1016/j.cclet.2021.09.013
1001-8417/

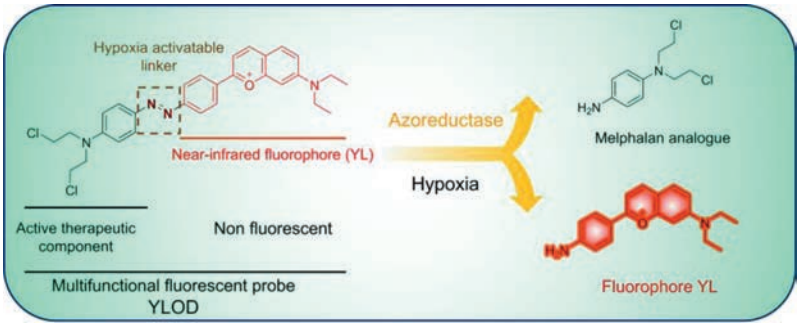

Scheme 1. Hypoxia fluorescent probe YLOD and its activation.

ery and release is constantly increasing. As near-infrared fluorescence has strong biological penetration, minimal damage to biological samples, and small background interference, it is very suitable for tumor monitoring in organisms [22,23]. Therefore, we focused our attention on designing and synthesizing multifunctional near-infrared fluorescent probes that can release anti-tumor drugs while detecting azoreductase in a hypoxia situation.

In this work, we report a near-infrared multifunctional fluorescent probe YLOD, consisting of three parts: the near-infrared fluorophore (YL), the azo bond, and the analogue of the anti-tumor drug melphalan. As shown in Scheme 1, YLOD showed no fluorescent signal under the normal oxygen environment. Once the azo bond was broken by reducing it with tin chloride or azo reductase, the fluorophore YL was released to generate a fluorescent emission at 620 nm. Through spectroscopic, cell, and animal experiments, we confirmed that YLOD was able to release the YL and the melphalan analogue in the presence of azoreductase in hypoxic environment, thus achieving hypoxia bioimaging and tumor treatment at the same time.

The multifunctional fluorescent probe YLOD was synthesized in two steps by the synthetic route displayed in Scheme S1 (Supporting information). Fluorophore YL was synthesized according to our previously reported methods [24]. YLOD was then obtained by diazo-coupling through YL and *N*,*N*-bis(2-chloroethyl)aniline. The synthetic and characterization (^{1}H NMR, ^{13}C NMR, and MS analysis) details of YLOD are given in Figs. S1–S3 (Supporting information).

In order to confirm that YLOD can release YL, we carried out spectroscopic experiments *in vitro*. Qian' group used tin chloride (reduced Sn^{2+}) to fracture the azo bond in the other azo group containing fluorescent probe [25]. First, we used reduced Sn^{2+} to confirm the occurrence of azo bond breakage and performed quan-

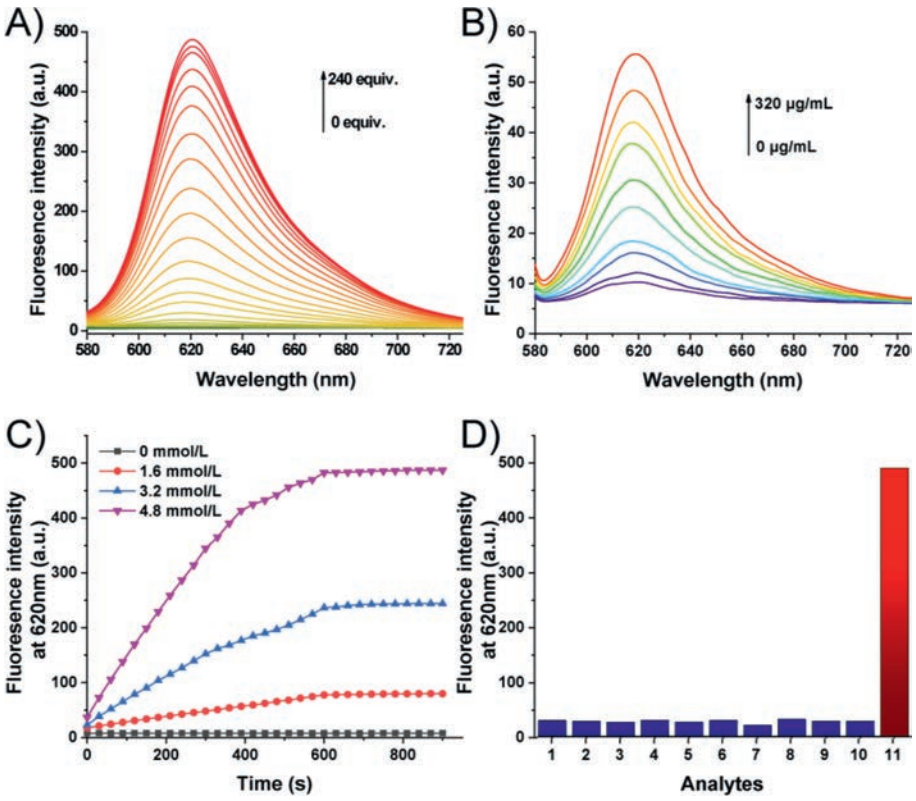

Fig. 1. (A) Fluorescence spectra of YLOD (20 μmol/L) in EtOH:PBS (ethanol:phosphate-buffered saline = 6/4 (v/v), pH 7.4) after adding different equivalents of Sn^{2+} (tin chloride). (B) Fluorescence spectra of YLOD (20 μmol/L) under different concentrations of rat liver microsomes (0–320 μg/mL) in PBS buffer (pH 7.4), containing 0.1 mmol/L NADH as a coenzyme. The spectra were recorded after incubation at 37 °C for 6 h in a hypoxic system. (C) Fluorescence intensity of YLOD (20 μmol/L) at 620 nm in the presence of varying concentrations of Sn^{2+} (0, 1.6, 3.2, and 4.8 mmol/L) in EtOH-PBS buffer system (6/4 (v/v), pH 7.4) as a function of varying time. (D) Fluorescence response of YLOD in the presence of various ions (1: GSH; 2: NO; 3: NO_2^-; 4: Vc; 5: HS^-; 6: HSO_4^-; 7: SO_3^{2-}; 8: H_2O_2; 9: $H_2PO_4^-$; 10: HPO_3^{2-}, 11: Sn^{2+}) at 620 nm (λ_{ex} = 565 nm).

titative analysis. As shown in Fig. 1A, with the addition of Sn^{2+}, the fluorescence value of YLOD at the maximum emission wavelength of 620 nm continued to increase. When the concentration of Sn^{2+} reached 240 equiv., the fluorescence intensity of YLOD no longer changed, and the test system reached saturation, turning the transition process from no fluorescence to red fluorescence. We also observed a similar phenomenon in YLOD treated rat liver microsomes, which were cytochrome P450 enriched vesicles and able to produce azoreductase in hypoxia [26]. As the concentration of rat liver microsomes increased, the fluorescence value of the prodrug YLOD kept rising (Fig. 1B). This result confirms that besides tin chloride, azoreductase from rat liver microsomes can also cause the breaking of the azo bond and release the fluorophore YL under hypoxic conditions.

In addition, we tested the time response of YLOD towards tin chloride, and the results are presented in Fig. 1C. The fluorescence intensity of probe YLOD increased over time and tended to stabilize around 10 min in different concentrations of Sn^{2+} systems. Fig. 1D shows a histogram of the fluorescence values of YLOD with each interfering ion at 620 nm. The fluorescence intensity of YLOD had no significant change after adding an equivalent amount of interfering ions in the reaction system. We also performed UV-vis spectroscopic experiments to further support the occurrence of azo bond breaking. As evident from Fig. S4 (in Supporting information), with the addition of Sn^{2+}, the 480 nm band of the probe YLOD red-shifted to 590 nm, and the resulting solution changed from orange-yellow to purple at this time. However, after adding the equivalent amount of interfering ions (GSH; NO; NO_2^-; Vc; HS^-; HSO_4^-; SO_3^{2-}; H_2O_2; $H_2PO_4^-$; HPO_3^{2-}) to the probe YLOD, the UV-vis spectra of the reaction system did not change significantly (Fig. S5 in Supporting information).

Next, the speculated mechanism was confirmed through ESI-MS analyses. When 240 equiv. of tin chloride was added to the YLOD solution (20 μmol/L), 2 signals in the mass spectrum were observed: the *m/z* value at 233.0601 corresponds to the melphalan analogue, and the other *m/z* value at 293.1653 indicates the fluorophore YL (Fig. S3 in Supporting information). This result again evidenced that the azo bond of YLOD could be cleaved to release the fluorophore YL and the melphalan analogue.

To further explore the effect of YLOD in tumor cells under the hypoxic environment, the cytotoxicity of YLOD on several cell lines with different oxygen levels was evaluated by MTT assay and melphalan analogue of *N,N*-bis(2-chloroethyl)aniline (MA) was selected as the control group. The experimental results are shown in Figs. 2A–D. It can be seen that inhibition of cell activity of all cell lines by YLOD was concentration-dependent. Compared with the normal oxygen environment, YLOD had a higher inhibition rate for tumor cells under the hypoxic environment, while the inhibition rate for human normal liver cells L02 had no significant difference whether it was normoxia or hypoxia (Figs. 2A and B). Contrarily, the inhibitory effect of MA on different cell lines at different oxygen levels did not vary considerably (Figs. 2C and D). These phenomena suggested that YLOD has tumor-targeting properties in the hypoxic environment. This might be attributed to the ability of YLOD to release more melphalan analogues in tumor cells by azoreductases under low-oxygen environments. Further, YLOD exhibited the strongest inhibitory effect on mouse breast cancer cells 4T1. At 1% O_2, the inhibition rate of 4T1 by YLOD (20 μmol/L)

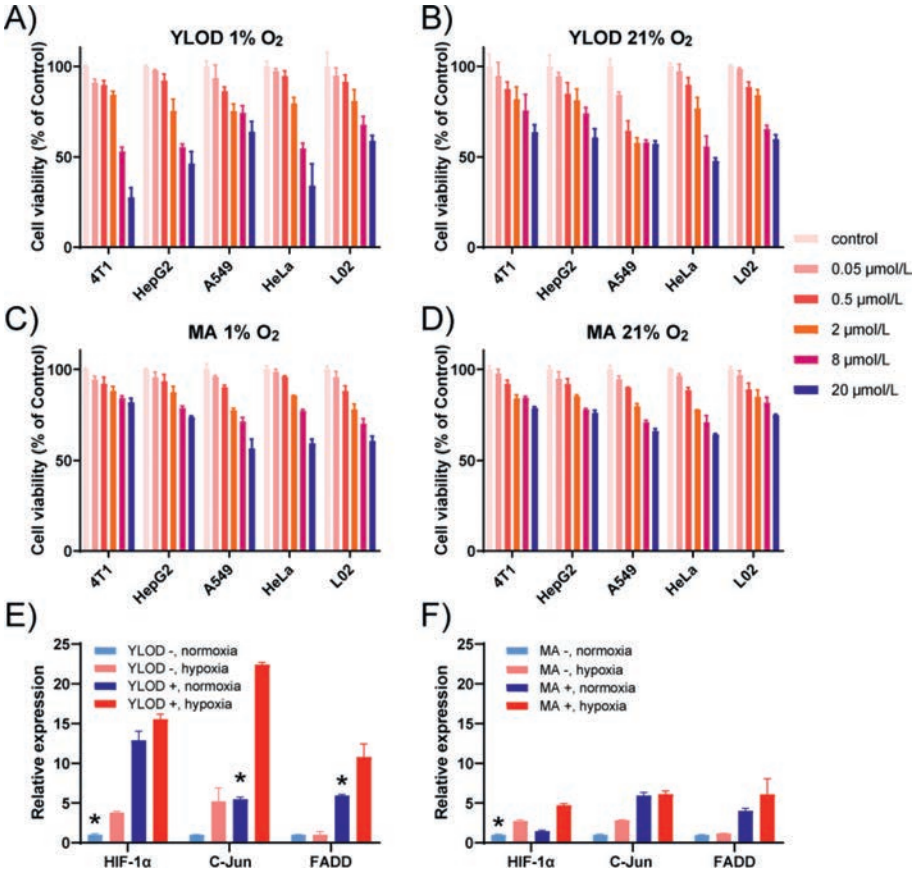

Fig. 2. Cytotoxicity of YLOD and MA under hypoxic and normoxic conditions. Cell viability of mouse breast cancer cells (4T1), liver hepatocarcinoma cells (HepG2), lung carcinoma cells (A549), cervical cancer cells (HeLa), and human normal liver cells (L02) upon treatment with various concentrations of YLOD under hypoxic (A) and normoxic (B) conditions. The above cell lines were treated with MA under hypoxic (C) and normoxic (D) conditions. After treatment, cells were incubated for 24 h. Cell viability was assessed by using a standard MTT assay. RT-qPCR results of HeLa treated with YLOD (E) and MA (F). $^*P < 0.05$.

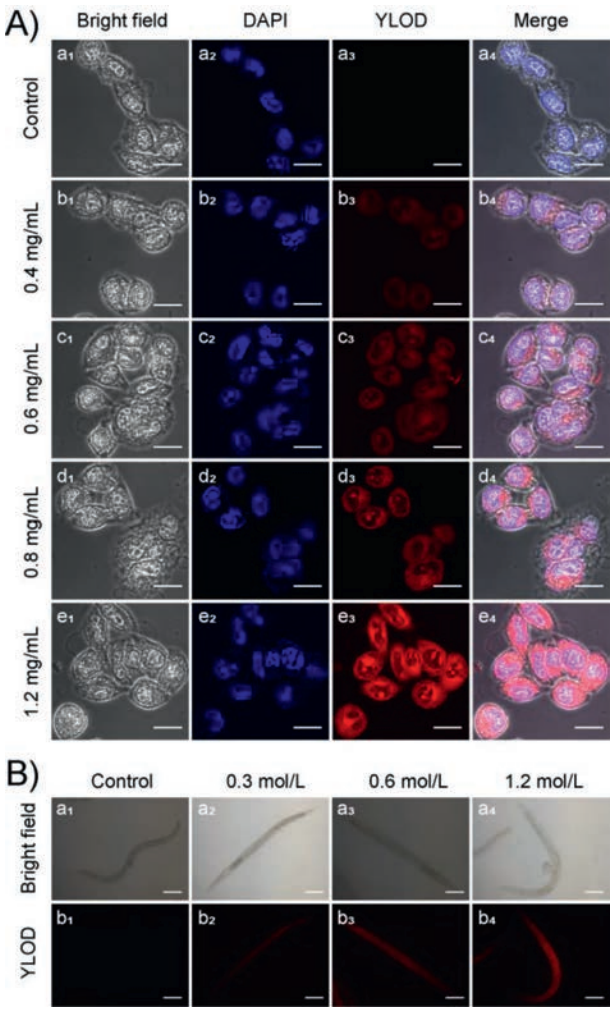

Fig. 3. (A) Confocal fluorescence images of HeLa cells, incubated in the PBS buffer solutions at different oxygen levels for 2 h. (a_1-a_4): only with YLOD (5 μmol/L); (b_1-b_4): with YLOD (5 μmol/L) and antioxidant (0.4 mg/mL); (c_1-c_4): with YLOD (5 μmol/L) and antioxidant (0.6 mg/mL); (d_1-d_4): with YLOD (5 μmol/L) and antioxidant (0.8 mg/mL); (e_1-e_4): with YLOD (5 μmol/L) and antioxidant (1.2 mg/mL). The first column shows bright-field images; the second column is blue channels, collected at 425–475 nm, stained with DAPI (4′,6-diamidino-2-phenylindole); the third column is red channels collected at 570–670 nm, stained with YLOD; last column is merged images of DAPI and YLOD. Scale bar: 20 μm. (B) Bright-field images (top) and fluorescence images (bottom) of *C. elegans*. (a_1, b_1): YLOD (10 μmol/L) only; (a_2, b_2): YLOD (10 μmol/L) and antioxidant NaN_3 (0.3 mol/L); (a_3, b_3): YLOD (10 μmol/L) and antioxidant; NaN_3 (0.6 mol/L); (a_4, b_4): YLOD (10 μmol/L) and antioxidant; NaN_3 (1.2 mol/L). Fluorescence images were collected in red channels. Scale bar: 100 μm.

reached 72.4%, much higher than 21% O_2. The semi-inhibition concentration of 4T1 by YLOD at 1% O_2 was 11.725 μmol/L. This suggested that 4T1 may be the cell line with the best effect of YLOD, and therefore 4T1 cell line was chosen for the tumor suppression experiments in nude mice.

RT-qPCR experiments of 4T1 cells were performed to confirm that YLOD can inhibit tumor cell activity by promoting the occurrence of cell apoptosis, and MA was set as the control group. The experimental results are displayed in Figs. 2E and F. The hypoxic environment can induce cells to express more hypoxia-inducible factor HIF-1α, a gene related to cellular hypoxia [27,28]. The expression of HIF-1α in 4T1 cells under hypoxia was observed higher than that under normoxia without YLOD or MA, confirming the success of hypoxia treatment (Figs. 2E and F). FADD and C-Jun are genes associated with apoptosis, with increased expression when apoptosis occurs [29,30]. YLOD significantly promoted the expression of FADD and C-JUN in 4T1 cells under hypoxia (Fig. 2E), suggesting it can promote tumor cell apoptosis. However, the effect of the MA group was not clear (Fig. 2F), further suggesting that YLOD was hypoxia-targeted to inhibit tumor cell growth. The results confirmed our prediction that YLOD could inhibit the growth of tumor cells by inducing apoptosis under hypoxia, indicating YLOD has the potential for tumor treatment.

Whether YLOD releases fluorophores in cells under oxygen deprivation remains unknown, but cell confocal imaging experiments can verify the presence of fluorophores. The antioxidant glutathione ethyl ester can induce the expression of azoreductase and other reductases in cells under a hypoxic environment [21]. We used glutathione ethyl ester in different concentrations (1.2 mg/mL, 0.8 mg/mL, 0.6 mg/mL, 0.4 mg/mL, and 0 mg/mL) to treat HeLa cells in vacuum for 2 h, and incubated with YLOD (5 μmol/L) for 2 h. After washing with PBS, observation by confocal microscope imaging and the experimental results are shown in Fig. 3A. It can be seen that with the increase of glutathione ethyl ester, the red fluorescence signal in HeLa cells enhanced, indicating the gradual increase of near-infrared fluorophore YL released by YLOD. The results demonstrated that YLOD could enter the cells and conduct localization imaging of azoreductase produced by external stimulation under hypoxia.

We also carried out fluorescence imaging experiments of *Caenorhabditis elegans* (*C. elegans*) to explore the imaging effect of YLOD. Sodium azide as an antioxidant can stimulate nematodes to express more azoreductase [31]. After adding sodium azide in different concentrations (0, 0.3, 0.6, and 1.0 mol/L) to *C. elegans* and followed by incubation with YLOD (10 μmol/L) for 2 h, fluorescence imaging was performed with a fluorescence microscope, and the results can be viewed in Fig. 3B. Similar to the cell imaging results, as sodium azide concentration increased, the red fluorescence signal in *C. elegans* gradually intensified, proving YLOD's utilization in monitoring the azoreductase produced by exogenously stimulated *C. elegans*.

Thus it is established that YLOD can be used to image the azoreductase produced by antioxidant stimulation in cells and *C. elegans*. Studying whether YLOD can image the endogenous expression of azoreductase induced by hypoxia in cells is therefore meaningful. We incubated HeLa cells under different oxygen levels (21%, 10%, and 1% O_2) for 12 h and then treated them with 5 μmol/L YLOD for 30 min. After washing them with PBS, we executed fluorescence imaging using a confocal fluorescence microscope. The experimental results are illustrated in Fig. 4A. Upon decreased oxygen content, the concentration of the near-infrared fluorophore YL escalated in HeLa cells, causing the red fluorescence signal to increase gradually. This result indicates the potential of YLOD to bioimage endogenous azoreductase induced by hypoxia in tumor cells. Combined with the previous results that YLOD could induce tumor cell apoptosis and inhibit the growth of tumor cells, we were convinced that YLOD could achieve targeted treatment of tumors.

In order to confirm this perception, tumor suppression experiments in nude mice were conducted. We selected BALB/c female mice and inoculated them with 4T1 cells, having the most pronounced inhibitory effect by YLOD in cell experiments. All animal studies were approved by the Committee on Animal Research and Ethics of Yunnan University (Yuncae2020303). Because the water solubility of YLOD is poor, we referenced the half-inhibitory concentration and chose the concentration of 1 mg/kg for experiments. One week after inoculation with 4T1 cells, YLOD was injected into nude mice through the tail vein; the administration period was 15 days, once every three days. After the administration period, to further explore the biological imaging capabilities of YLOD, we conducted imaging experiments on anatomical tumors and organs from mice. We dissected the tumor, heart, liver,

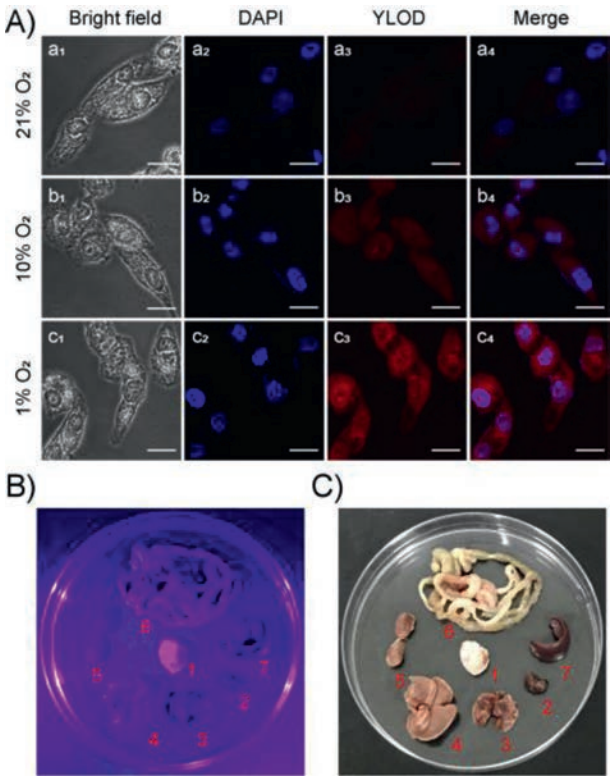

Fig. 4. (A) Confocal fluorescence images of HeLa cells, cultured with different oxygen contents (1%, 10%, and 21%) for 10 h before imaging. Incubated in the PBS buffer solutions with YLOD (5 μmol/L) for 30 min. The first column shows bright-field images; the second column is the blue channel, stained with the nuclear stain from Hoechst (collected at 425–475 nm); the third column is the red channel collected at 570–670 nm; the last column is merged images. Scale bar: 20 μm. (B and C) Representative images of dissected organs of nude mice bearing 4T1-induced tumors: (B) ultraviolet light (λ_{ex} = 370 nm), (C) solar light. The mice were sacrificed, and organs were removed and incubated with 20 μmol/L of YLOD for 2 h under hypoxic conditions. 1: 4T1 tumor; 2: heart; 3: lung; 4: liver; 5: kidney; 6: intestine; 7: spleen. For interpretation of the references to color in this figure legend, the reader is referred to the web version of this article.

spleen, lung, kidney, and intestines of mice, incubated them with 20 μmol/L YLOD for 2 h, and took photos under ultraviolet light (λ_{ex} = 370 nm, Fig. 4B) and solar light (Fig. 4C). It is clear from Figs. 4B and C that only the tumor displayed a strong purple fluorescent signal. This result signifies that YLOD has good targeting and bioimaging capabilities. Dissected tumors of the test group were found to be significantly smaller than the control group (Fig. 5A), and the weight of the tumors from the test group was also significantly less compared to the control group (Fig. 5B). Body weights of the mice did not change much during the experiment period (Fig. 5C), implying that YLOD was not toxic to mice. During the administration period, there was a significant reduction in the volume of the tumors in the test group compared to the control group (Fig. 5D). Hence, it can be concluded that YLOD can target and inhibit tumor growth in 4T1-cells inoculated xenograft murine mouse model. Thus, the outcomes of tumor suppression experiments confirmed our previous hypothesis that YLOD possesses the ability of tumor-targeted therapy.

In conclusion, we have developed a new hypoxia-targeted near-infrared multifunctional fluorescent probe YLOD, which responded to azoreductase to release near-infrared fluorophore and the analogue of the anti-tumor drug melphalan. The whole process was accompanied by a red fluorescence increase at 620 nm, which enabled the dynamic imaging observation of the hypoxia degree in cancer cells and tissues. In a hypoxic environment, the released anti-tumor drugs promoted apoptosis of tumor cells and inhibited

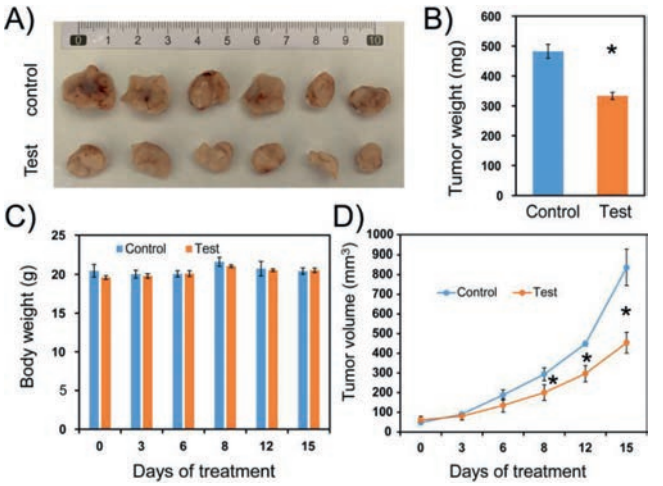

Fig. 5. *In vivo* therapeutic effects of YLOD. (A) Dissected tumor tissue image of mice treated with PBS (control) and 1 mg/kg (test) of YLOD in DMSO after 15 days (n = 3 per group). (B) Tumor weight and (C) body weights of mice during the experiment. (D) Tumor volume change of two groups. Note that all treatments were tail-vein injected every three days, for 15 days. $^{*}P < 0.05$.

the growth of tumors in nude mice. As a multifunctional fluorescent probe, YLOD successfully visualized the hypoxic region of the tumors and synchronized tumor treatment *in situ*, demonstrating its clinical potential for future oncotherapy.

Declaration of competing interest

The authors declare that they have no known competing financial interests or personal relationships that could have appeared to influence the work reported in this paper.

Acknowledgments

This work is supported by the National Natural Science Foundation of China (No. 22067019), China-Sweden Joint Mobility Project (No. 51811530018) and the Scientific Research Foundation Project of Yunnan Provincial Department of Education (No. 2021Y031). Authors thank Advanced Analysis and Measurement Center of Yunnan University for the sample testing service.

Supplementary materials

Supplementary material associated with this article can be found, in the online version, at doi:10.1016/j.cclet.2021.09.013.

References

[1] R.L. Siegel, K.D. Miller, A. Jemal, CA Cancer J. Clin. 69 (2019) 7–34.
[2] R.L. Siegel, K.D. Miller, H.E. Fuchs, et al., CA Cancer J. Clin. 71 (2021) 7–33.
[3] L. Wu, Y. Sun, K. Sugimoto, et al., J. Am. Chem. Soc. 140 (2018) 16340–16352.
[4] D. Yue, M. Wang, F. Deng, et al., Chin. Chem. Lett. 29 (2018) 648–656.
[5] J. Li, Z. Su, C. Yu, et al., Dyes Pigm. 192 (2021) 109451.
[6] T. Cao, L. Zhang, H. Ma, et al., Sens. Actuators B: Chem. 338 (2021) 129841.
[7] Z. Chai, D. Liu, X. Li, et al., Chem. Commun. 57 (2021) 5063–5066.
[8] Y. Zhao, S. Wu, J. Wu, et al., Cancer Biol. Ther. 11 (2011) 95–107.
[9] L.B. Harrison, M. Chadha, R.J. Hill, et al., Oncologist 7 (2002) 492–508.
[10] J. Cummings, V.J. Spanswick, M. Tomasz, et al., Biochem. Pharmacol. 56 (1998) 405–414.
[11] P. Vaupel, L. Harrison, Oncologist 9 (2004) 4–9.
[12] S. Kizaka-Kondoh, H. Konse-Nagasawa, Cancer Sci. 100 (2009) 1366–1373.
[13] Y. Zhou, K.N. Bobba, X.W. Lv, et al., Analyst 142 (2017) 345–350.
[14] D. Yang, H.Y. Tian, T.N. Zang, et al., Sci. Rep. 7 (2017) 9174.
[15] X. Li, J. Wang, R. Cui, et al., Dyes Pigm. 179 (2020) 108395.
[16] M. Gao, F. Yu, C. Lv, et al., Chem. Soc. Rev. 46 (2017) 2237–2271.
[17] C. Yan, L. Shi, Z. Guo, et al., Chin. Chem. Lett. 30 (2019) 1849–1855.
[18] R. Kumari, D. Sunil, R.S. Ningthoujam, et al., Chem. Biol. Interact. 307 (2019) 91–104.

[19] J. Jantsch, D. Chakravortty, N. Turza, et al., J. Immunol. 180 (2008) 4697–4705.
[20] X. Tian, Z. Li, Y. Sun, et al., Anal. Chem. 90 (2018) 13759–13766.
[21] Y. Zhou, M. Maiti, A. Sharma, et al., J. Control. Release 288 (2018) 14–22.
[22] C. Yan, Y. Zhang, Z. Guo, Coordin. Chem. Rev. 427 (2021) 213556.
[23] X. Jiang, L. Rong, J. Cao, et al., Dyes Pigm. 191 (2021) 109375.
[24] L. Yu, P. Verwilst, I. Shim, et al., CCS Chem. 2 (2020) 2725–2739.
[25] Q. Cai, T. Yu, W. Zhu, et al., Chem. Commun. 51 (2015) 14739–14741.
[26] O. Tangen, J. Jonsson, S. Orrenius, Anal. Biochem. 54 (1973) 597–603.
[27] C.J. Hu, L.Y. Wang, L.A. Chodosh, et al., Mol. Cell. Biol. 23 (2003) 9361–9374.
[28] Y.H. Pan, X.X. Chen, L. Dong, et al., Chin. Chem. Lett. 32 (2021) 3895–3898.
[29] R. Wisdom, R.S. Johnson, C. Moore, EMBO J. 18 (1999) 188–197.
[30] W.C. Yeh, J.L. de la Pompa, M.E. McCurrach, Science 279 (1998) 1954–1958.
[31] F. Gao, P. Okunieff, Z. Han, et al., Adv. Exp. Med. Biol. 566 (2005) 249–256.